358, 302 (1992); A. Miranker, C. V. Robinson, S. E. Radford, R. T. Aplin, C. M. Dobson, *Science* **262**, 896 (1993).
24. G. Wildegger and T. Kiefhaber, *J. Mol. Biol.* **270**, 294 (1997).
25. S. A. Woodson and T. R. Cech, *Biochemistry* **30**, 2042 (1991).
26. D. E. Draper, *Trends Biochem. Sci.* **21**, 145 (1996); D. Thirumalai and S. A. Woodson, *Accounts Chem. Res.* **29**, 433 (1996); K. A. Dill and S. Chan, *Nature Struct. Biol.* **4**, 10 (1997).
27. M. S. Rook, D. K. Treiber, J. R. Williamson, in preparation.
28. For each mutant, the fraction of active molecules at 37°C was determined by measuring the kinetic burst in a multiple-turnover cleavage assay as described [D. Herschlag and T. R. Cech, *Biochemistry* **29**, 10159 (1990)]. In all instances, the active ribozyme concentration was nearly equal to the total ribozyme concentration. This result was obtained whether the ribozymes were prefolded in either 10 or 2 mM Mg^{2+}, indicating that the mutations do not markedly destabilize the final, active conformation.
29. We thank P. Kim and B. Tidor for reviewing the manuscript, J. W. Orr for assistance with Fig. 2, and T. R. Cech for providing A186U plasmid DNA. Supported by the Rita Allen Foundation, the Alfred P. Sloan Foundation, and the Camille and Henry Dreyfus Foundation (J.R.W.). D.K.T. was supported by an American Cancer Society postdoctoral fellowship and P.P.Z. by a Howard Hughes Medical Institute predoctoral fellowship.

29 August 1997; accepted 4 February 1998

Energy Transduction on the Nanosecond Time Scale: Early Structural Events in a Xanthopsin Photocycle

Benjamin Perman, Vukica Šrajer, Zhong Ren, Tsu-yi Teng, Claude Pradervand, Thomas Ursby, Dominique Bourgeois, Friederich Schotte, Michael Wulff, Remco Kort, Klaas Hellingwerf, Keith Moffat*

Photoactive yellow protein (PYP) is a member of the xanthopsin family of eubacterial blue-light photoreceptors. On absorption of light, PYP enters a photocycle that ultimately transduces the energy contained in a light signal into an altered biological response. Nanosecond time-resolved x-ray crystallography was used to determine the structure of the short-lived, red-shifted, intermediate state denoted [pR], which develops within 1 nanosecond after photoelectronic excitation of the chromophore of PYP by absorption of light. The resulting structural model demonstrates that the [pR] state possesses the *cis* conformation of the 4-hydroxyl cinnamic thioester chromophore, and that the process of *trans* to *cis* isomerization is accompanied by the specific formation of new hydrogen bonds that replace those broken upon excitation of the chromophore. Regions of flexibility that compose the chromophore-binding pocket serve to lower the activation energy barrier between the dark state, denoted pG, and [pR], and help initiate entrance into the photocycle. Direct structural evidence is provided for the initial processes of transduction of light energy, which ultimately translate into a physiological signal.

Elaborate systems exist in a wide variety of species to gather light energy and convert it into chemical energy or into a structural signal that ultimately leads to a biological response. The structural bases for these conversions are not well understood. The initial chemical step associated with photoactivity is often photoisomerization of a highly conjugated protein prosthetic group that may generate an altered signaling conformation. This is subsequently recognized by a diffusible or other messenger that delivers the signal to downstream effectors (*1*). The best studied example is the generation of the meta II state of mammalian sensory rhodopsin by photoisomerization of its opsin chromophore and the subsequent activation of several molecules of transducin during the long half-life of the meta II intermediate (*2*). We describe the early structural changes that occur upon absorption of light in a member of a particularly simple class of bacterial photoreceptors: the xanthopsins (*3*).

The xanthopsin from the photoautotrophic purple eubacterium *Ectothiorhodospira halophila*, known as photoactive yellow protein (PYP), is a small, 14-kD, water-soluble protein in which a 4-hydroxy cinnamic acid chromophore is covalently linked through a thioester to the γ sulfur of Cys^{69} (*4*). PYP appears to serve as the initial response generator in *E. halophila* for a light-initiated signaling cascade that leads ultimately to a negative phototactic response (*5*). The biochemical and genetic details of this signal transduction process are, at present, unknown.

The chromophore is stabilized in the *trans* configuration as the phenolate anion in the binding pocket of the dark-state protein, denoted pG (Figs. 1 and 2A). The chromophore is completely buried with no atom exposed to solvent (*6*). These properties contribute to the protein's characteristic absorption peak at a wavelength of 446 nm (*4*, *7*, *8*). Upon photoelectronic excitation, PYP efficiently enters a fully reversible photocycle that contains at least two spectrally distinct intermediate states, denoted [pR] and [pB], each presumably associated with structural changes in the chromophore and its protein environment (Fig. 1). The rate constants for interconversion of the intermediate states progressively decrease throughout the photocycle (*7*), and therefore, the presumed signaling state [pB] accumulates under constant illumination that populates a saturated photostationary state (*9*). Time-resolved x-ray crystallographic studies with 10-ms time resolution of the decay from this photostationary state confirm that the chromophore is in the *cis* conformation (*10*) as predicted by chemical studies (*11*). The decay was shown to involve ejection of the chromophore from its binding pocket, displacement of the side chain of Arg^{52} that closes the chromophore-binding pocket, exposure of the chromophore to the solvent, its protonation (*10*, *12*), and concomitant major rearrangement of the H-bond network that stabilized the phenolate anion in the dark state (*6*, *13*). The chemical and crystallographic studies so far have not identified the stage in the photocycle at which chromophore isomerization occurs, probed earlier structural changes in the photocycle, or indicated how the [pB] state is generated. These ultrafast structural changes in PYP that ultimately lead to the formation of the [pB] state are critical to its function as a photoreceptor.

The recent development of nanosecond time-resolved x-ray crystallography (*14*, *15*) provides the opportunity to study the processes leading to the formation of the [pB] state in crystals of PYP (*16*) and, hence, to characterize early structural intermediates. The experiments were conducted at the white beamline ID-9 at the European Synchrotron Radiation Facility (ESRF), Grenoble, France, in a manner closely similar to that used to study ligand photolysis, rebinding, and protein relaxation in carbonmonoxy myoglobin (*14*, *15*). The photocycle was initiated by delivery of a focused, unpolarized,

B. Perman, Department of Biochemistry and Molecular Biology, University of Chicago, Chicago, IL 60637, USA. V. Šrajer, Z. Ren, T.-y. Teng, C. Pradervand, K. Moffat, Department of Biochemistry and Molecular Biology and the Consortium for Advanced Radiation Sources, University of Chicago, Chicago, IL 60637, USA.
T. Ursby, Molecular Biophysics, Chemical Center, Lund University, Post Office Box 124, S-221 00 Lund, Sweden. D. Bourgeois, F. Schotte, M. Wulff, European Synchrotron Radiation Facility, 38043 Grenoble Cedex, France. R. Kort and K. Hellingwerf, Laboratory for Microbiology, E. C. Slater Institute, 1018 WS Amsterdam, Netherlands.

*To whom correspondence should be addressed. E-mail: moffat@cars.uchicago.edu

7-ns laser pulse [full width at half maximum (FWHM)] at 495 nm to small crystals at 287 K (*17*, *18*). The structure was probed at a series of time delays after the laser pulse, ranging from 1 ns to 1 ms, by an x-ray pulse of 150 ps duration (ESRF single-bunch mode) or a pulse train of 1.8 μs duration (ESRF 2/3-filling hybrid mode). Diffraction from the small crystals used in the experiment (*17*) was weak, and the structural signal expected was small (*18*). Complete x-ray data sets were therefore collected with roughly 14-fold redundancy and 10-fold averaging of each individual image (*17*) to yield accurate structure factor amplitudes and to permit outlier identification (Table 1).

We present results obtained at the shortest time delay of 1 ns that reveal the earliest intermediate in the photocycle identifiable with the current methodology. We associate this intermediate with the [pR] state. Structure factor amplitudes derived from Laue intensities were used to calculate a difference Fourier map with coefficients $|F|_{1\ ns} - |F|_{dark}$ that reveals the structural differences between the earliest intermediate, [pR], and the dark, pG states (Fig. 3). The difference map contoured at 2.6σ [where σ is the root-mean-square (rms) value of the difference electron density in the entire asymmetric unit] shows prominent features that are, as expected, largely confined to the local environment of the chromophore (Fig. 3). The lack of any features on the aromatic moiety of the chromophore (Fig. 3) is, however, unexpected and indicates that this moiety remains buried and that its center does not undergo significant translational motion in the transition to the [pR] state. Several prominent features in the difference map indicated specific changes in the positions of atoms of the chromophore and its local environment (Fig. 3).

We built several trial models for the [pR] state that sought to account for these features. Only one accounted for features in omit maps in which the chromophore is omitted. This model could also be successfully refined against the Laue data (Table 2) (*19*). Care had to be taken in refining a short-lived, unstable structure against such a small signal in the data, particularly because the standard protein parameters used in crystallographic refinement are derived from un-

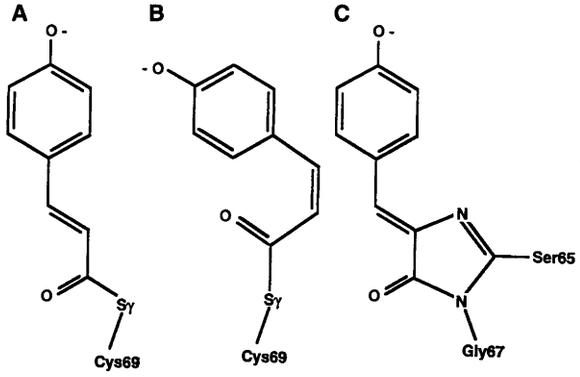

Fig. 2. The chromophore disposition in pG (**A**) and [pR] (**B**) is compared with the chromophore of GFP (**C**) (*32*), formed by posttranslational autocatalytic conversion of Ser^{65}, Tyr^{66}, and Gly^{67} to 4-(4-hydroxybenzylidene)-imidazolidin-5-one (*24*).

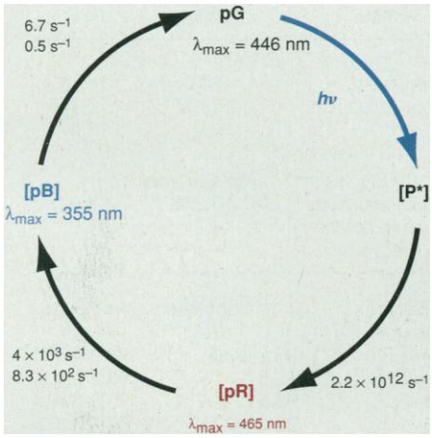

Fig. 1. The PYP photocycle. Upon absorption of blue light, the electronic excited state of the chromophore, [P*], is generated by a transition from π to π* in the conjugated system. Thermal relaxation from this electronic excited state to the first intermediate state, [pR] (*31*), is accompanied by a red shift of the absorption maximum (*7*). Biphasic thermal relaxation yields the second intermediate state, [pB], with a substantial blue shift in the absorption maximum (*7*). The photocycle is completed by protein-assisted, thermal, *cis*-to-*trans* reisomerization that recovers the dark state, pG (*7*, *11*). The biphasic nature of the interconversion between states suggests that thermal relaxation occurs via multiple pathways and that the intermediate states are structurally heterogeneous (*9*). Therefore, we represent these states by square brackets: [P*], [pR], and [pB]. This figure displays the essential features of the photocycle; however, more complicated models can be envisaged.

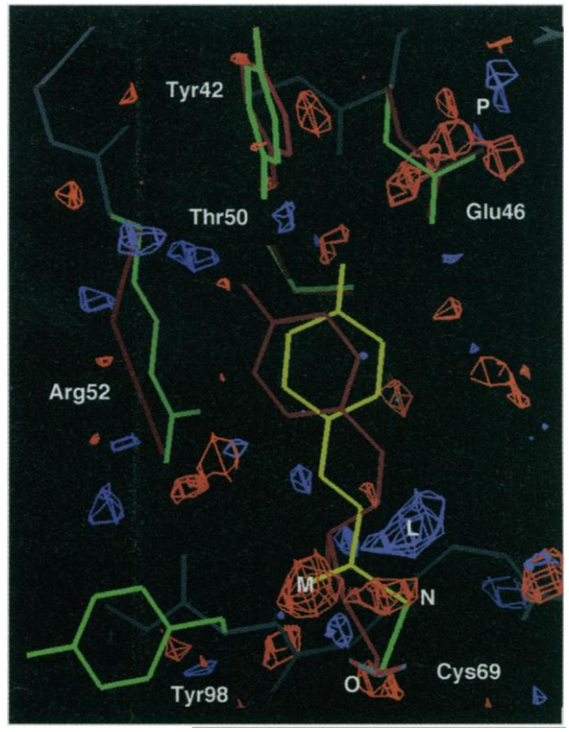

Fig. 3. $|F|_{1\ ns} - |F|_{dark}$ difference Fourier map. The 1-ns difference map is superimposed on the pG structure (*6*) with important side chains in green and the chromophore in yellow. The model for the 1-ns structure is also shown in maroon. The difference features exceeding 2.6σ are shown as basket-weave contours. Blue and red contours indicate regions of positive and negative difference electron density, respectively. The most prominent positive feature (+5.0σ; denoted L) appears to result from repositioning of the vinyl C atoms of the chromophore. It is associated with negative features on the chromophore carbonyl O (–5.6σ; denoted M) and the γ S of Cys^{69} (–4.6σ; denoted N) that together indicate motion of these atoms. These data suggest that a "crankshaft" motion of the chromophore tail occurs upon isomerization that does not require a flip of its aromatic moiety; the initial structural changes in the chromophore are then seen mainly in its tail. Another prominent negative feature (–3.8σ; denoted O) below the α C of Cys^{69} suggests that the backbone in this proximal region (*20*) of the chromophore pocket shifts toward the chromophore. Such a backbone motion is required if the aromatic moiety at the opposite, or distal, end of the chromophore is pinned. *Trans*-to-*cis* isomerization must cause a contraction of around 0.5 Å in the overall chromophore length (as measured by the distance from the Cys^{69} γ S to the phenolate O). A further set of features is associated with atoms of the distal region of the chromophore-binding pocket, near the phenolate moiety. Feature "P" on the ε_1 side chain O of Glu^{46} indicates its motion toward Tyr^{42} and perhaps an increase in its temperature factor.

strained stable structures and may not be directly applicable to short-lived structures. The model that was successfully refined contained a *cis* conformation about the chromophore vinyl π bond created through (i) torsion about the Cys^{69} χ_1 and χ_2 dihedral angles associated with the bond between the γ sulfur and the chromophore carbonyl C; (ii) minor changes in the proximal (*20*) polypeptide backbone dihedral angles; and (iii) torsion about the χ_1 and χ_2 dihedral angles of the side chains of Tyr^{42} and Glu^{46} (Figs. 2B and 4B). That is, *trans* to *cis* isomerization was completed in less than 1 ns. The chromophore remains in its binding pocket. The center of its aromatic moiety does not move, although the ring has rotated in its plane. The chromophore retains its H-bond to the hydroxyl of Tyr^{42}, which is slightly displaced. The Thr^{50} hydroxyl also shifts to maintain its role as the H-bond donor to the hydroxyl of Tyr^{42}. The side chain of Glu^{46} shifts away from Tyr^{42} toward the protein core. The distance between a Glu^{46} side chain O and the phenolate O increases to >5 Å and demonstrates that the H-bond in pG to the chromophore phenolate O has been broken in the [pR] state. Glu^{46} appears not to form a stronger H-bond to the phenolate of the chromophore at this stage of the photocycle, in contrast to the interpretation of Fourier-transform infrared spectroscopy difference spectra obtained at 70 K in D_2O (*13*). Our finding is more consistent with results from the $Glu^{46} \rightarrow Gln^{46}$ mutant (*21*), in which the rate of the [pR]-to-[pB] transition is increased despite the inability of Gln to serve as a proton donor. No new H-bond associated with the side chain of Glu^{46} can be identified in the [pR] state; however, Glu^{46} may remain stabilized by longer range electrostatic interactions with ionized groups in other regions of the protein.

The rotation of the aromatic moiety of the chromophore in its plane moves the phenolate O toward the side chain of Arg^{52} (Fig. 4B). In the saturated photostationary state, the side chain of Arg^{52} moves away from the chromophore and opens the binding pocket "hatch" (*6*, *10*). The refinement of the [pR] state shows that the guanidinium group of Arg^{52} moves about 0.7 Å out of the chromophore pocket toward the solvent, consequently lengthening the H-bonds between its guanidinium group and the carbonyl Os of Tyr^{98} and Thr^{50}. Its bond to Tyr^{98} represents the only direct link between the distal and proximal portions of the binding pocket other than those associated with the chromophore itself.

Photoisomerization disrupts the distal H-bonding network of the phenolate in [pR] and requires that the α and β carbons of Cys^{69} move toward the chromophore to maintain stabilization of the phenolate anion by the H-bond to the Tyr^{42} hydroxyl. This motion of the proximal main chain atoms is

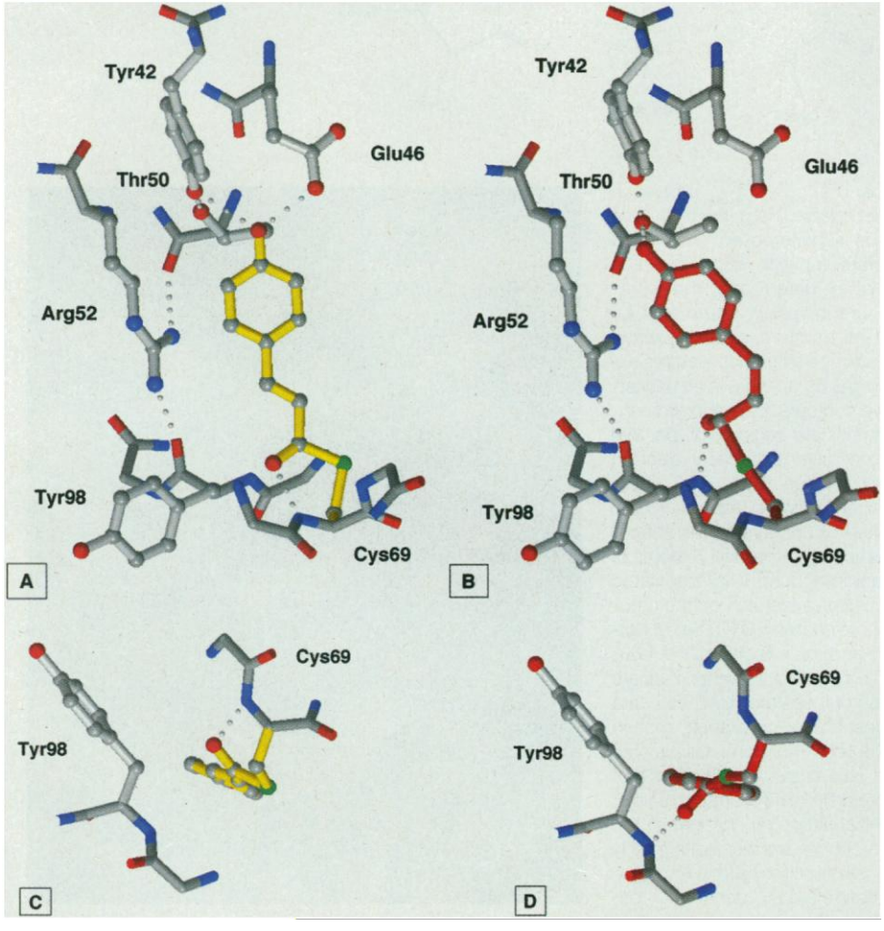

Fig. 4. Comparison of the pG and [pR] state structures: the chromophore and its environment are viewed in the pG structure (*6*) (**A**) and the refined structure of the [pR] state (**B**). In (C) and (D), the chromophore and the Cys^{69} and Tyr^{98} residues are viewed from the proximal end of the binding pocket. The pG (**C**) and [pR] state (**D**) differ in the position of the tail carbonyl O with respect to the plane of the conjugated system of the chromophore. The distance from the carbonyl O to the amide N of Cys^{69} is 2.69 Å in pG; the distance from the carbonyl O to the amide N of Tyr^{98} is 2.83 Å in [pR]. The distance between the amide Ns of Cys^{69} and Tyr^{98} remains fixed at 6.07 Å in both pG and [pR].

Table 1. Crystallographic data collection and reduction. PYP_{dark} and $PYP_{1\ ns}$ refer to data taken before or after the laser pulse. For $PYP_{1\ ns}$, the laser/x-ray pulse had a delay of 1 ns.

Item	PYP_{dark}	$PYP_{1\ ns}$
Singles		
Observations	190,053	182,155
Unique reflections*	10,475	10,475
R_{merge} on F^2 (%)†	12.8	13.4
R_{merge} on $\|F\|$ (%)‡	9.2	9.2
Singles and multiples combined		
Unique reflections*	13,376	13,027
Overall redundancy	14.2	14.0
$R_{dark/1\ ns}$ (%)§	—	6.7

Resolution range (Å)‖	Completeness (%)¶	
∞–3.00	93.2 (93.2)	93.2 (93.2)
3.00–2.38	95.3 (94.2)	95.3 (94.2)
2.38–2.08	93.5 (94.0)	93.5 (94.0)
2.08–1.90	92.0 (93.5)	92.0 (93.5)
1.90–1.75	89.7 (92.7)	90.0 (92.8)
1.75–1.65	86.7 (91.7)	87.0 (91.8)
1.65–1.57	71.5 (88.8)	71.8 (89.0)
1.57–1.50	45.3 (83.4)	44.8 (83.4)

*Unique reflections with $F/\sigma_F > 2$, where σ_F is the rms deviation determined from merging of structure amplitudes. †$R_{merge} = \Sigma|F^2 - \langle F^2\rangle|/\Sigma F^2$, where F^2 is the square of the structure factor amplitude of an observed reflection, calculated by scaling the integrated intensity by a general scale factor, and $\langle F^2\rangle$ is the mean from multiple observations and symmetry-related measurements. ‡$R_{merge} = \Sigma\||F| - \langle|F|\rangle|/\Sigma|F|$, where $|F|$ is the structure factor amplitude $\langle|F|\rangle$ is the average amplitude from multiple observations. §$R_{dark/1\ ns} = \Sigma\||F|_{dark} - S\cdot|F|_{1\ ns}|/\Sigma|F|_{dark}$, where $|F|_{dark}$ and $|F|_{1\ ns}$ are the observed structure factor amplitudes for PYP_{dark} and $PYP_{1\ ns}$, respectively, and S is the scaling factor. ‖All data were integrated to 1.5 Å resolution; however, only the data to 1.9 Å were used in structural refinement. ¶Completeness by resolution shells for singles and multiples combined. Cumulative completeness is also shown in parentheses. Binning is based on equal shell volume.

accompanied by breaking of the H-bond between the chromophore carbonyl O and the amide group of Cys^{69}. In [pR], the carbonyl C of the chromophore tail adopts a highly strained, pseudo-sp3 geometry (Fig. 4, B and D). The H-bond between the carbonyl O of the chromophore tail and the amide group of Cys^{69} is broken in [pR] as the carbonyl reorients and forms a new H-bond with the backbone amide group of Tyr^{98}. In pG, the carbonyl O of the chromophore tail lies above the conjugated plane of the chromophore (Fig. 4C), near the Cys^{69} amide group. In [pR], the O is on the other side of the ring, H-bonded to the backbone amide group of Tyr^{98} (Fig. 4D). The carbonyl O cannot lie in the plane of the chromophore ring in the *cis* isomer without severe energetic penalties due to substantial steric hindrance between the O and ring Hs. In the saturated photostationary state representing [pB], the carbonyl O reforms its H-bond with the amide group of Cys^{69} (*10*); thus, the transition from [pR] to [pB] must traverse this high energy barrier. This provides a structural explanation for why the interconversion from [pR] to [pB] is much slower than the interconversion from [P*] to [pR] (*7*).

The regions of the backbone that move in the transition from pG to the [pR] state largely correspond to regions of nonideal secondary structure in pG. Helix C, in the distal region of the chromophore-binding pocket, is underwound at its COOH-terminal end, as evident in long backbone H-bond distances of >3.2 Å between Glu^{46} and Thr^{50} and Gly^{47} and Gly^{51}, which indicates that the backbone of helix C is strained in pG. The proximal backbone adjacent to Cys^{69} is also flexible. The main chain between Ala^{67} and Thr^{70} forms two overlapping type III β turns (*22*) that have elongated, main chain H-bond distances and nonideal backbone dihedral angles. The second β turn also overlaps with a single turn of π helix, identified by a canonical H-bond between the main chain carbonyl O of Thr^{70} and the amide of Tyr^{76}. The proximal and distal regions are the sole sites of protein backbone motion between the pG and [pR] states. The lack of strong interresidue main chain H-bonds in pG evidently provides PYP with the necessary flexibility in critical regions to permit the substantial structural changes that must accompany isomerization in a chromophore that is buried and completely solvent-inaccessible in its binding pocket. This feature plays a pivotal role in establishing an accessible free-energy pathway between the dark state and subsequent intermediates in the photocycle upon excitation with blue light.

Table 2. Crystallographic refinement of the [pR] state.

Item	Value
Atoms per asymmetric unit	1168
Refined atomic positions	54
Residues per asymmetric unit	125
Residues with alternate conformation*	14
Residues with refined alternate conformation*	7
Final dark-state occupancy†	0.85
Final 1 ns light-state occupancy†	0.15
R_{cryst}‡	0.180
R_{free}	0.185

*Residues with alternate conformations include those from the original structure determination of pG and those corresponding to the [pR] state. Only the [pR] alternate conformations were refined. †The final occupancies are normalized such that they add to unity. ‡R_{cryst} denotes the standard crystallographic R factor: $hkl\Sigma\|F_{obs(hkl)}| - s|F_{calc(hkl)}\|/hkl\Sigma F_{obs(hkl)}$, where $F_{obs(hkl)}$ and $F_{calc(hkl)}$ are the observed and calculated structure factor amplitudes of a reflection with indices h, k, l, and s is a scale factor.

The flexibility in the chromophore and its protein environment is quite different in green fluorescent protein (GFP) from *Aequorea victoria*. Despite a strong similarity in the chromophore structure of the two proteins (*23*), the tail of the GFP chromophore is covalently locked in its conformation and evidently lacks the flexibility of the PYP chromophore and its binding pocket (Fig. 2C). GFP does not have a photocycle like PYP, but converts the energy of the absorbed photon into highly efficient fluorescence emission. Several mutants of GFP derive enhanced fluorescence quantum yields from further restriction of the conformational flexibility of the chromophore region (*24*), thus hindering a thermal relaxation pathway and increasing fluorescence emission. In contrast, PYP has a low fluorescence quantum yield ($\sim 10^{-3}$) (*25*) and a high quantum yield for entering the photocycle ($Q = 0.35$) (*7*, *26*). Flexible parts of the chromophore and its binding pocket in PYP may direct specific changes in conformation, thus allowing efficient entrance into a photocycle that provides a thermal means for dissipation of energy, whereas rigidity in the GFP chromophore and its binding pocket hinders changes in conformation and enhances fluorescence. If significant fluorescence is to occur, stabilizing structural elements must inhibit changes in conformation that would otherwise occur within the lifetime of the electronic excited states.

Strain in the chromophore itself is offset largely by maintaining the H-bonding networks that stabilize the polar atoms of the chromophore in the different conformations observed in pG and [pR]. Because the [pR] state involves conformational changes that lead to highly specific reordering of the H-bonds between the protein and the chromophore, [pR] may itself be a signaling state, and not merely an obligatory precursor to the long-lived and, hence, presumptive signaling state, [pB]. Although the half-life of [pR] is probably too short to bind diffusible second messenger molecules, there may be another PYP ligand in the signal transduction system that binds pG and has a substantially reduced affinity for [pR]. On formation of [pR], the ligand would be quickly released. Such a molecule may, by binding pG in the dark, play a role in photocycle quenching similar to the arrestin and rhodopsin kinase quenching pathway in mammalian sensory rhodopsin (*27*).

The structure of PYP in the dark is cocked and ready for structural changes. Light provides the large amount of energy to promote isomerization, and thus pulls the trigger.

REFERENCES AND NOTES

1. H. G. Khorana, *J. Biol. Chem.* **267**, 1 (1992).
2. S. Yarfitz and J. B. Hurley, *ibid.* **269**, 14329 (1994).
3. R. Kort *et al.*, *EMBO J.* **15**, 101 (1996).
4. W. D. Hoff *et al.*, *Biochemistry* **33**, 13959 (1994); M. Baca *et al.*, *ibid.*, p. 14369.
5. W. W. Sprenger, W. D. Hoff, J. P. Armitage, K. J. Hellingwerf, *J. Bacteriol.* **175**, 3096 (1993).
6. G. E. O. Borgstahl, D. R. Williams, E. D. Getzoff, *Biochemistry* **34**, 6278 (1995).
7. W. D. Hoff *et al.*, *Biophys. J.* **67**, 1691 (1994); T. E. Meyer, *Biochim. Biophys. Acta* **806**, 175 (1985).
8. A. R. Kroon *et al.*, *J. Biol. Chem* **271**, 31949 (1996).
9. K. Ng, E. D. Getzoff, K. Moffat, *Biochemistry* **34**, 879 (1995).
10. U. K. Genick *et al.*, *Science* **275**, 1471 (1997).
11. R. Kort *et al.*, *FEBS Lett.* **382**, 73 (1996).
12. M. Kim, R. A. Mathies, W. D. Hoff, K. J. Hellingwerf, *Biochemistry* **34**, 12669 (1995).
13. A. Xie, W. D. Hoff, A. R. Kroon, K. J. Hellingwerf, *ibid.* **35**, 14671 (1996).
14. D. Bourgeois *et al.*, *J. Synchrotron Radiat.* **3**, 65 (1996).
15. V. Šrajer *et al.*, *Science* **274**, 1726 (1996).
16. Overproduction, purification, and crystallization of PYP. *Apo*PYP was obtained at the University of Amsterdam, by heterologous overproduction in *Escherichia coli* M15/pHisp, and was purified as described (*3*). Reconstitution with 4-hydroxy cinnamic anhydride was carried out as described [Y. Imamoto, T. Ito, M. Kataoka, F. Tokunaga, *FEBS Lett.* **374**, 157 (1995)]. After dialysis against 50 mM tris-HCl (pH 7.5), the histidine-tagged holoPYP sample was incubated for 18 hours with enterokinase at a ratio of 1:1000 (w/w) at 37°C to remove the histidine tag and then applied to a ResourceQ anion exchange column. Eluted holoPYP fractions were concentrated and washed with 10 mM tris-HCl (pH 7.5), using a 10-kD cut-off concentrator (Amicon), followed by lyophilization for storage and shipment to the University of Chicago. Samples of lyophilized PYP were dissolved in 20 mM phosphate buffer, 100 mM NaCl (pH 7), and further purified on an HR 16/50 S-100 gel filtration column (Pharmacia, Piscataway, NJ). Pure fractions (optical purity < 0.45) were collected, concentrated, and crystallized using methods modified from (*10*). The crystals were nearly identical to those used (*6*) in the determination of the pG structure: space group $P6_3$ with unit-cell dimensions of $a = b = 66.9$ Å and $c = 40.8$ Å (determined by LaueView).
17. Data acquisition and processing. Small (80 μm by 80 μm by 150 μm) crystals were excited using single 4-mJ laser pulses (7 ns FWHM, ≤1.5-mm-diameter beam cross section at the crystal, 495-nm wavelength) from a coumarin 500-dye laser (Continuum) pumped by the third harmonic of a Nd:YAG laser (Continuum) timed to arrive at specified times (between 1 ns and 1 ms) in advance of a single x-ray pulse or pulse train. This delay is defined as the time from the peak of the laser pulse to the edge of the x-ray pulse (*14*). A 70-pole wiggler and a

hybrid 46-pole undulator (wavelength range of 0.3 to 1.8 Å) were used simultaneously to further enhance the x-ray intensity at the crystal. Single x-ray pulses were isolated with a microsecond shutter train (*14*) from the ESRF storage ring operating in single-bunch mode at a machine current of 15 mA. Laue diffraction intensities were collected on an image-intensified charge-coupled device detector (Thompson; ESRF). To minimize systematic errors such as those related to x-ray absorption, we collected a dark data set for each crystal in addition to the photoexcited data sets. Data sets consist of 30 images taken at crystal angular settings separated by 2° through a range of 60°. Each image is a composite of 10 150-ps exposures accumulated on the detector before readout, to enhance the relatively weak diffraction data collected in single-bunch mode. No significant radiation damage was detected over the course of data collection. Data were reduced and scaled with the LaueView software package (*28*). Laue reflections stimulated by several energies (multiples) were successfully deconvoluted and included in the final data set, which improved the completeness at low resolution and the overall redundancy.

18. Extent of photoinitiation. Optical thickness directly affects the extent of photoexcitation in the crystal. Crystals that are too thick will have a lower extent of photoinitiation and a highly nonuniform excitation throughout their volume (*9*). With 7-ns laser pulses at longer wavelengths, the possibility of photoexcitation of molecules in the [pR] state is encountered, which may stimulate reisomerization of the [pR] state back to pG. We demonstrated (V. Šrajer and B. Perman, unpublished results) that the photocycle can be successfully initiated in the crystal under our experimental conditions, and estimate that 12% of the molecules are converted to the [pB] state.
19. Crystallographic refinement. The 1-ns model was refined against the Laue data limited to 1.9 Å resolution to minimize the influence of error in the integrated intensities at higher resolutions, for which I/σ_I is low. All refinement processes used X-PLOR, version 3.851 (*29*). The crystallographic refinement was restricted to only those residues that, according to inspection of the $|F|_{1\ ns} - |F|_{dark}$ difference Fourier map and of several simulated annealing (SA) omit maps, appear to move in response to photoinitiation. The atomic positions refined are those of the chromophore; the three proximal residues Pro^{68}, Cys^{69}, and Thr^{70}; and the distal side chains of Tyr^{42}, Glu^{46}, Thr^{50}, and Arg^{52}. Once these atoms were identified, a difference refinement strategy (*30*) was used in least-squares minimization of the residual between observed and calculated differences in structure factor amplitudes. This approach gave improved estimates of structural differences by reducing model-error terms. The chromophore refinement parameters incorporate information on the energetics of isomerization of the vinyl bond and charge distribution across the conjugated system of the chromophore (F. Zhou and P. Bash, personal communication). The energy function for rotation about the vinyl bond is given by $E_{DIHEDRAL} = k_{180}(1 - \cos\delta) + k_0(1 + \cos\delta)$, where δ is the phase shift angle, k_{180} = 750 kcal mol^{-1} rad^{-2} for the *trans* conformer (ϕ_i = 180°), and k_0 = 500 kcal mol^{-1} rad^{-2} for the *cis* conformer (ϕ_i = 0°). This relationship gives a two-well sinusoidal potential surface for isomerization about the vinyl bond that has wells of different depths. The deeper well is centered at 180° and corresponds to the *trans* conformer; the shallow well is centered at 0° and corresponds to the *cis* conformer. Difference refinement and inspection of SA omit maps were repeated for several occupancy values (10, 15, and 20%) for the extent of photoinitiation in crystals in the range anticipated from microspectroscopic measurements (*18*). A random 10% sample of the data was retained for use in calculation of R_{free}. Coordinates for the [pR] state of PYP have been deposited in the Brookhaven Protein Data Bank under accession code 2pyr.
20. The term "proximal" is used to denote regions of the chromophore binding pocket near Cys^{69}; the term "distal" refers to regions at the opposite end of the pocket near Tyr^{42}.
21. U. Genick *et al.*, *Biochemistry* **36**, 8 (1997).
22. P. Y. Chou and G. D. Fasman, *J. Mol. Biol.* **115**, 135 (1977); C. M. Wilmot and J. M. Thornton, *ibid.* **203**, 221 (1988); J. S. Richardson, *Adv. Protein Chem.* **34**, 167 (1981). Only the type III β turn can exist as an overlapped pair because of a special pattern in the main-chain dihedral angles, where $\phi_{i+1} = \phi_{i+2}$ and $\psi_{i+1} = \psi_{i+2}$.
23. F. Yang, L. G. Moss, G. N. Phillips Jr., *Nature Biotechnol.* **14**, 1246 (1996); M. Ormö *et al.*, *Science* **273**, 1392 (1996).
24. R. Heim, A. D. Cubitt, R. Y. Tsien, *Nature* **373**, 663 (1995).
25. T. E. Meyer, G. Tollin, T. P. Causgrove, P. Cheng, R. E. Blankenship, *Biophys. J.* **59**, 988 (1991); W. D. Hoff, S. L. S. Kwa, R. Van Grondelle, K. J. Hellingwerf, *Photochem. Photobiol.* **56**, 529 (1992).
26. M. E. Van Brederode, T. Gensch, W. D. Hoff, K. J. Hellingwerf, S. E. Braslavsky, *Biophys. J.* **68**, 1101 (1995).
27. K. Palczewski, *Protein Sci.* **3**, 1355 (1994).
28. Z. Ren and K. Moffat, *J. Appl. Crystallogr.* **28**, 461 (1995); *ibid.*, p. 482.
29. A. T. Brünger, J. Kuriyan, M. Karplus, *Science* **235**, 458 (1987); A. T. Brünger, A. Krukowski, J. W. Erickson, *Acta Crystallogr. A* **46**, 585 (1990).
30. T. C. Terwilliger and J. Berendzen, *Acta Crystallogr. D* **51**, 609 (1995).
31. H. Chosrowjan, N. Mataga, N. Nakashima, Y. Imamoto, F. Tokunaga, *Chem. Phys. Lett.* **270**, 267 (1997); A. Baltuska *et al.*, *ibid.*, p. 263.
32. R. Heim, D. C. Prasher, R. Y. Tsien, *Proc. Natl. Acad. Sci. U.S.A.* **91**, 12501 (1994).
33. We thank R. Cordfunke for expert assistance in the preparation of PYP samples, M. Roth for use of the pulsed laser, S. Labouré for laser technical assistance, and W. Schildkamp for participation in time-resolved x-ray crystallographic technique development. K.M. thanks D. McRee and E. Getzoff for introducing him to PYP. Supported by grants from NIH to K.M.

24 November 1997; accepted 23 February 1998

Mutation in Transcription Factor *POU4F3* Associated with Inherited Progressive Hearing Loss in Humans

Oz Vahava,* Robert Morell,* Eric D. Lynch,* Sigal Weiss, Marjory E. Kagan, Nadav Ahituv, Jan E. Morrow, Ming K. Lee, Anne B. Skvorak, Cynthia C. Morton, Anat Blumenfeld, Moshe Frydman, Thomas B. Friedman, Mary-Claire King, Karen B. Avraham†

The molecular basis for autosomal dominant progressive nonsyndromic hearing loss in an Israeli Jewish family, Family H, has been determined. Linkage analysis placed this deafness locus, *DFNA15*, on chromosome 5q31. The human homolog of mouse *Pou4f3*, a member of the POU-domain family of transcription factors whose targeted inactivation causes profound deafness in mice, was physically mapped to the 25-centimorgan DFNA15-linked region. An 8–base pair deletion in the POU homeodomain of human *POU4F3* was identified in Family H. A truncated protein presumably impairs high-affinity binding of this transcription factor in a dominant negative fashion, leading to progressive hearing loss.

The inner ear is a complex structure requiring a large repertoire of genes to orchestrate sound acquisition and vestibular function on many levels, including neuronal innervation, structural integrity, and mechanoelectrical transduction. Although as many as 100 genes may be involved (*1*), only a small number of genes have been identified that cause nonsyndromic hearing loss: human connexin 26 (*GJB2*) (*2*), human myosin VIIA (*MYO7A*) (*3*), human diaphanous (*4*), and mouse myosin VI (*Myo6*) (*5*). Another POU-domain transcription factor, *POU3F4* (POU domain, class 3, transcription factor 4), causes human X-linked mixed deafness, DFN3 (*6*).

We are studying the genetic basis of progressive hearing loss in an Israeli Jewish family. The family traces its ancestry to Italy and to subsequent migrations through various North African and Middle Eastern countries, including Tunisia, Libya, and Egypt, with branches of the family now living in Israel, the United States, and Belgium (*7*). Five generations demonstrate autosomal dominant inheritance of progressive deafness (Fig. 1A). The earliest record

O. Vahava, S. Weiss, M. E. Kagan, N. Ahituv, K. B. Avraham, Department of Human Genetics, Sackler School of Medicine, Tel Aviv University, Tel Aviv 69978, Israel.
R. Morell and T. B. Friedman, National Institute on Deafness and Other Communication Disorders (NIDCD), National Institutes of Health, Bethesda, MD 20850, USA.
E. D. Lynch, J. E. Morrow, M. K. Lee, M.-C. King, Departments of Medicine and Genetics, University of Washington, Seattle, WA 98195, USA.
A. B. Skvorak and C. C. Morton, Department of Pathology and Department of Obstetrics, Gynecology, and Reproductive Biology, Brigham and Women's Hospital and Harvard Medical School, Boston, MA 02115, USA.
A. Blumenfeld, Unit for Development of Molecular Biology and Genetic Engineering, Hadassah University Hospital, Mt. Scopus, Jerusalem 91240, Israel.
M. Frydman, Genetics Institute, Haim Sheba Medical Center, Tel Hashomer 52621, Israel, and Department of Human Genetics, Sackler School of Medicine, Tel Aviv University, Tel Aviv 69978, Israel.

*These authors contributed equally to this report.
†To whom correspondence should be addressed. E-mail: karena@post.tau.ac.il